International Journal of Nanomedicine

Dovepress
open access to scientific and medical research

Open Access Full Text Article

ORIGINAL RESEARCH

Designing Green Synthesis-Based Silver Nanoparticles for Antimicrobial Theranostics and Cancer Invasion Prevention

Taghrid S Alomar[1], Najla AlMasoud[1], Manal A Awad[2], Reem S AlOmar[3], Nada M Merghani[4], Mohamed El-Zaidy[5], Ajaya Bhattarai[6]

[1]Department of Chemistry, College of Science, Princess Nourah Bint Abdulrahman University, Riyadh, 11671, Saudi Arabia; [2]King Abdullah Institute for Nanotechnology, King Saud University, Riyadh, 11451, Saudi Arabia; [3]Department of Family and Community Medicine, College of Medicine, Imam Abdulrahman Bin Faisal University, Dammam, 32210, Saudi Arabia; [4]Central Research Laboratory, Vice Rectorate for Studies and Scientific Research, King Saud University, Riyadh, 11451, Saudi Arabia; [5]Department of Botany and Microbiology, Faculty of Science, King Saud University, Riyadh, 11459, Saudi Arabia; [6]Department of Chemistry, Mahendra Morang Adarsh Multiple Campus, Tribhuvan University, Biratnagar, 56613, Nepal

Correspondence: Ajaya Bhattarai; Manal A Awad, Email ajaya.bhattarai@mmamc.tu.edu.np; mawad@ksu.edu.sa

Introduction: Researchers are increasingly favouring the use of biological resources in the synthesis of metallic nanoparticles. This synthesis process is quick and affordable. The current study examined the antibacterial and anticancer effects of silver nanoparticles (AgNPs) derived from the *Neurada procumbens* plant. Biomolecules derived from natural sources can be used to coat AgNPs to make them biocompatible.

Methods: UV-Vis spectroscopy was used to verify the synthesis of AgNPs from *Neurada procumbens* plant extract, while transmission electron microscopy (TEM), photoluminescence (PL) spectroscopy, dynamic light scattering (DLS), and Fourier transform infrared spectroscopy (FTIR) were used to characterize their morphology, crystalline structure, stability, and coating.

Results: UV-visible spectrum of AgNPs shows an absorption peak at 422 nm, indicating the isotropic nature of these nanoparticles. As a result of the emergence of a transmission peak at 804.53 and 615.95 cm^{-1} in the spectrum of the infrared light emitted by atoms in a sample, FTIR spectroscopy demonstrated that the Ag stretching vibration mode is metal-oxygen (M-O). Electron dispersive X-ray (EDX) spectral analysis shows that elementary silver has a peak at 3 keV. Irradiating the silver surface with electrons, photons, or laser beams triggers the illumination. The emission peak locations have been found between 300 and 550 nm. As a result of DLS analysis, suspended particles showed a bimodal size distribution, with their Z-average particle size being 93.38 nm.

Conclusion: The findings showed that the antibacterial action of AgNPs was substantially ($p \leq 0.05$) more evident against *Gramme-positive strains (S. aureus and B. cereus)* than *E. coli*. The biosynthesis of AgNPs is an environmentally friendly method for making nanostructures that have antimicrobial and anticancer properties.

Keywords: Silver nanoparticles, UV-Vis spectroscopy, transmission peak, dynamic light scattering

Introduction

The oxidation/reduction process of metallic ions by the organic biological moiety is used in the green production of nanoparticles (NPs). The green and convenient synthesis of silver nanoparticles (AgNPs) is a bottom-up technique.[1] It includes the treatment of silver nitrate solution with reducing substances using extracts derived from plants. The gold NPs are mixed with silver nitrate solution following the standard operating procedure explained earlier.[2] The most common synthesis methods in green chemistry are hydro(solvo)thermal synthesis, ball milling, ultrasoundassisted sonochemical synthesis, microwave irradiation, photocatalysis, magnetic field-assisted synthesis, solvents, and catalysis.[3] Compared to physical and chemical methods, nanoparticles produced using green technology have many advantages. For example, green synthesis reduces chemical costs and energy consumption. It also generates environmentally benign products and by-products,[4] including fungi, algae, bacteria, and plants. It is important to note that there has

Received: 18 September 2023
Accepted: 9 March 2024
Published: 21 May 2024

been widespread criticism of the excessive use of plant components such as leaves, fruits, roots, stems, and seeds in the production of NPs.[5] Many scientists now choose green synthesis over conventional chemical and physical approaches because it is toxic-free, zero-pollution, eco-friendly, cost-effective, safer, and more sustainable.[2–6] There are, however, some things about this method that could be improved.

Silver nanoparticles are presently being evaluated as potentially useful anticancer treatments because they affect the cell cycle, inhibit the multiplication of cancer cells, produce oxidative stress, and promote the process of programmed cell death (apoptosis).[7]

As silver nanoparticles and their conjugates with anticancer medicines produce reactive oxygen species (ROS) and oxidative stress, DNA damage occurs, cell cycle arrest occurs, and tumor cells die.[8,9]

The actions of silver nanoparticles as an antimicrobial agent involve: 1) Nanoparticles of silver produce silver ions (Ag+) that disrupt cell walls and cytoplasmic membranes 2) By denaturing ribosomes, silver ions inhibit protein synthesis.[10] The antimicrobial properties of AgNPs derived from plant extracts have been demonstrated to suppress both Gram-negative and Gram-positive bacteria.[11] In green synthesis, harmful chemicals are eliminated. Both reducing and capping agents may be found in plants.[12] Moreover, eco-friendly green synthesised nanoparticles using medicinal plants are crucially important because of their potential therapeutic uses.[13,14]

Previously, the potential of biogenic AgNPs as cancer theranostic agents and their underlying processes were investigated.[15] Interest in cancer research has surged because of AgNPs due to their easy manufacturing and surface modification, significant increases, and better biocompatibility.[16,17] Over the last decade, researchers have focused their attention on developing strategies for synthesizing AgNPs using biological and green chemical processes.[18] A study was conducted to enhance in vivo environmental biocompatibility of silver nanoparticles (AgNPs) by functionalizing them with lipopeptide biosurfactant extracted from Brevibacterium casei LS14.[19] Based on the study's findings, biosurfactants could be used to functionalize AgNP so that it could be used in biomedical and environmental applications. A variety of nanoparticles modified to have unique physical, chemical, structural, electrical, and magnetic properties have gained recognition in advancing nanobiotechnology, including biomedicine, sensors, and wastewater management.[20] By using a unique combinatorial approach based on first-principles density functional theory and simulations, the research shed light on the role of diverse AgNPs-protein interactions, thus paving the way for understanding their intrinsic properties.[21] The study evaluated the anti-proliferative and apoptotic properties of AgNPs biofabricated from Microchaete aqueous extract.[22]

Seeds of wheat and corn were germinated in water or soil with different doses of irradiation, and the paramagnetic centers in their seedlings were compared. Research pertaining to the formation of inorganic nanophase magnetic particles in biological systems is of great importance for the development of the field of biomineralization.[23] Silver nanoparticles were synthesized using aqueous extracts of chickpea (*Cicer arietinum L.*) (CA) leaves. X-ray diffraction (XRD), FTIR, UV-visible spectrophotometer, TEM, SEM, EDX, and zeta potential (ZP) were used to analyze the synthesized AgNPs.[24]

It was found that olive leaf extracts could be used to synthesize silver nanoparticles where absorption peak occurred between 405 nm and 425 nm. The SEM images was shown the spherically-shaped Ag-NPs with polydisperse and size range of 7.12 to 18.8 nm.[25]

In 2020, there was a study of green synthesis of Ag-NPs from *Neurada procumbens* where a strong absorption maximum occurred between 400 and 455 nm for Ag-NPs fabricated using *Neurada procumbens* extract.The TEM and SEM images demonstrated the existence of spherically-shaped Ag-NPs with a size range of 20 to 50 nm. The Ag-NPs shown effective efficacy against the isolated multi-drug resistant gram-negative rod from suspected patients at Buraidah Central Hospital, Saudi Arabia when tested against bacterial cultures.

The highest concentration of Ag-NPs that could be obtained ranged from 75 to 100 µg, with a 15–17 mm zone of inhibition.[26]

The current research aims to utilize *Neurada procumbens* as an eco-friendly plant to prepare AgNPs. Additionally, the low bioavailability of *Neurada procumbens* may be countered by using AgNPs as a carrier. AgNPs conjugated with *Neurada procumbens* are being studied for their possible cytotoxic and anticancer impact for microbial theranostics and ameliorative effect against cancer invasion. To this end, UV-visible spectrum, PL spectrum, DLS, TEM micrographs, EDX, and FTIR are used.

Methods and Materials

Reagents and Materials

Both pure rifaximin and rifaximin in the form of gastrobiotic tablets, each containing 550 mg of rifaximin, were provided by the Al Andalous Medical Company, Egypt. Boric acid with (99.5%), citric acid (99.5%), and acetic acid (99.7%) were all available from the company Winlab, United Kingdom. Furthermore, sodium tetraborate decahydrate (99.99%), sodium acetate (99.99%), sodium monobasic phosphate (99.99%), sodium citrate dihydrate (99.99%), sodium dibasic phosphate (99.99%), silver nitrate (99.99%), and ethanol (99.82%) were purchased from Sigma-Aldrich, Germany.

Preparation of AgNPs Using an Aqueous Neurada Procumbens Flora Extract

The *Neurada procumbens* plant samples were collected from the Almuzahemiah region near Riyadh in February 2019, and identified by Dr. Mohamed El-Zaidy in the Herbarium, Department of Botany and Microbiology, King Saud University (KSU). A voucher specimen (No.: JC20190210) was stored at the Research Laboratory, Department of Chemistry, College of Science, Princess Nourah bint Abdulrahman University, Riyadh, Saudi Arabia.

After being air-dried, the leaves of *Neurada procumbens* were macerated overnight at room temperature in a mixture of double-distilled hot water at a ratio of 1:10. This mixture was continually shaken. The obtained extract was filtered. After that, about 5 mL of the aqueous leaf extracts were combined with 50 mL of 1.0 mM $AgNO_3$. After heating the reaction mixtures to 60 °C and stirring them constantly until the color changed from clear to brown (about one hour), the color was changed into brown. In order to keep the nanoparticles from clumping together, the mixing container was taken off the stirrer after the solution achieved its maximum color intensity and placed in the dark at room temperature. The formation of silver nanoparticles was demonstrated by the color change (Scheme 1).

MTT Assay

Dimethyl sulfoxide (DMSO), crystal violet, and trypan blue dye were procured from Sigma (St. Louis, Mo., USA), while Fetal Bovine serum, DMEM, RPMI-1640, HEPES buffer solution, L-glutamine, gentamicin, and 0.25% Trypsin-EDTA

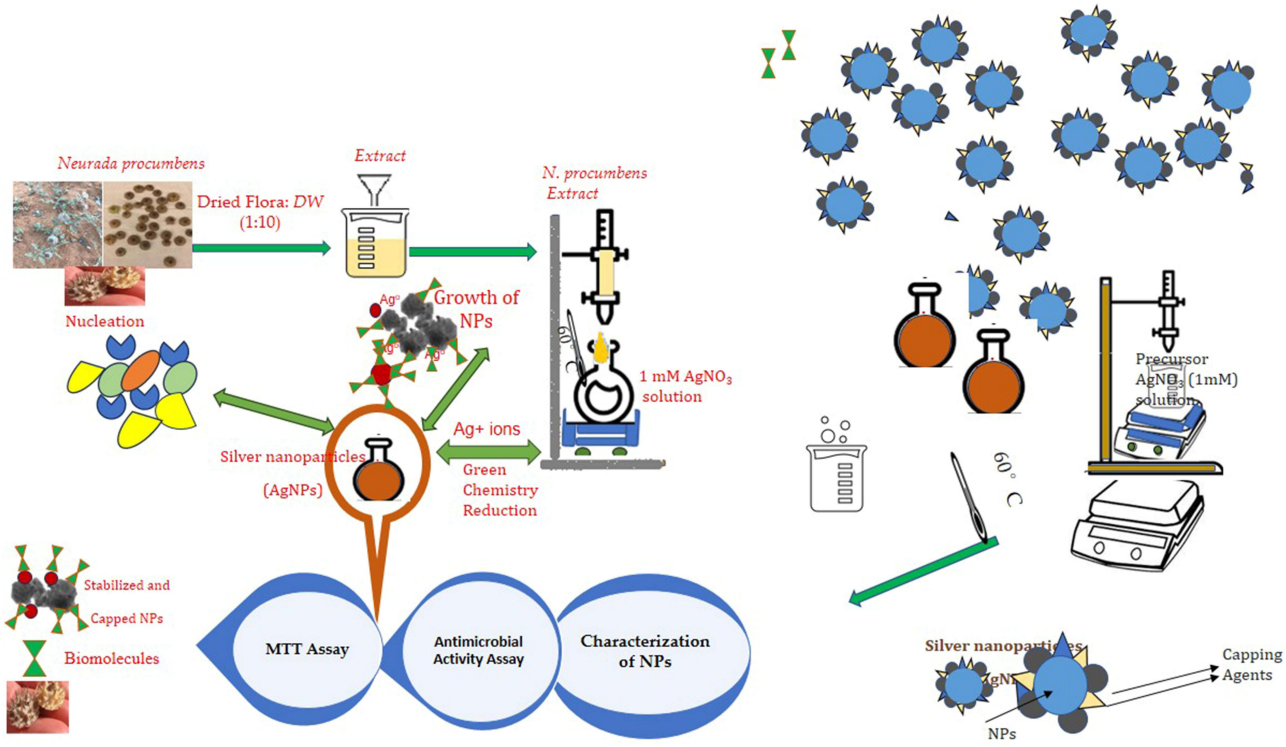

Scheme 1 An illustration of the AgNPs' route of synthesis utilizing Neurada procumbens Flora extract.

were sourced from Bio Whittaker ® Lonza, Belgium. The Hela (human cervical cancer cells) obtained from American Type Culture Collection, USA, whereas the MCF-7 cells (human breast cancer cell line) were obtained from VACSERA Tissue Culture Unit. The cells lines were grown in a CO_2 incubator at 37 °C for 24 h after being seeded at a density of 30×10^4 per well in µL of cell culture media. After incubation, media in 96-well plates were discarded, and cells were exposed to plant extract + NPs with culture medium in concentrations of (0, 1, 2, 4, 8, 24, 48, and 80) µg/mL. Then, 96 wells were incubated for a whole day in a CO_2 incubator at 37 °C. The MTT powder was diluted in PBS at a pH of 7.4 to 5 mg/mL, and 20 L was added to each well. The plates were then incubated at 37 °C for 3h. Following incubation, cells were rinsed in PBS, and DMSO (200 L/well) was added to dissolve the formazan crystals. For 15 minutes at room temperature, the plates were incubated on a shaker to achieve thorough dissolution. At 570 nm, the absorbance of each sample was evaluated with the assistance of a microplate reader manufactured by Synergy-HI: BioTek, USA.

Antimicrobial Activity Assay

14gm of Nutrient Agar powder were dissolved in 500 mL of distilled water and autoclaved afterwards. The agar was poured in 20mL for each Petri dish. The researchers waited 15 minutes for the agar to solidify, and then plates were swabbed with the overnight culture of human pathogens: *Escherichia coli* ATCC 35218; from the King Khalid University Hospital in Riyadh, Saudi Arabia, obtained *Staph aureus* ATCC 43300, Enterococcus faecalis ATCC 29212, and Bacillus cereus ATCC 11778 (clinical isolate).

A well was made in the solid medium by carefully punching it with a sterile cork borer (four wells per plate), and each of the four corners was an equal distance away from the dish's center. After that, the hole was filled with the material in three different concentrations (1000 L, 500 L, and 250 L), which were introduced carefully until the hole was saturated. The mixture was then incubated for 24 h at 37 °C. After incubation, the zone of inhibition was measured and outlined as a millimeter (mm) in diameter.

Fusarium oxysporum, Alternaria alternate, and Trichoderma were used to test the extracts' antifungal efficacy. These fungi were cultured on a plate of Potato Dextrose Agar at a temperature of 28 °C. The 19 grams of medium in 500 mL of distilled water were autoclaved before use. The material was diluted to two different quantities (1000 µL and 500 µL), added, and then put onto sterile petri plates with gentle mixing. A 6-mm-diameter fungal disc was removed from the edge of the fungus cultures that were 7 days old. It was then aseptically placed on the poisoned plate and cultured for 7 days at 28 °C to test this theory.

The diameter of the fungal colonies was measured, and the percentage of mycelia growth inhibition was used to determine the antifungal activity. The inhibition % was assessed on 7th day, when the mycelia in the control plate had extended to the edge of the Petri dish.

Results and Discussion

In the presence of plant extracts, it would be able to see the color shift and follow the reduction of silver ions to AgNPs using spectroscopic techniques. *N. procumbens* was used to create AgNPs, first validated by the reaction solution's color shift from almost colorless to yellowish and eventually brown. This effect was seen as a result of AgNPs' surface plasmon vibration resonance being excited.[27]

The UV-Vis spectrum of formed AgNPs showed a single absorption at 422 nm which is matched with the literature[26] (Figure 1). This indicates an isotropic nature of these nanoparticles[27] due to the resonance of excited longitudinal plasmon vibrations in a sample solution of AgNPs. This highlights Mie's theory, which proposes that asymmetry in a sphere causes the longitudinal plasmon resonance to expand and redshift and the transverse plasmon resonance to arise.[28–30] Several studies have shown that the presence of a sharp SPR in the range of 350–600 nm confirms the formation of colloidal silver nanoparticles, while others have reported that the surface plasmon resonance of AgNPs at wavelengths of 410–450 nm may indicate spherical nanoparticles.[31–33] The synthesised Ag NPs have a broader asymmetric band in their UV spectra, with one peak and one shoulder toward long wavelengths. This might provide evidence for size distribution and the existence of larger NPs, as postulated by Mishra et al.[34] Aggregation effects may have contributed to this expansion. It has also been shown that the strength, width, and form of the absorption band are

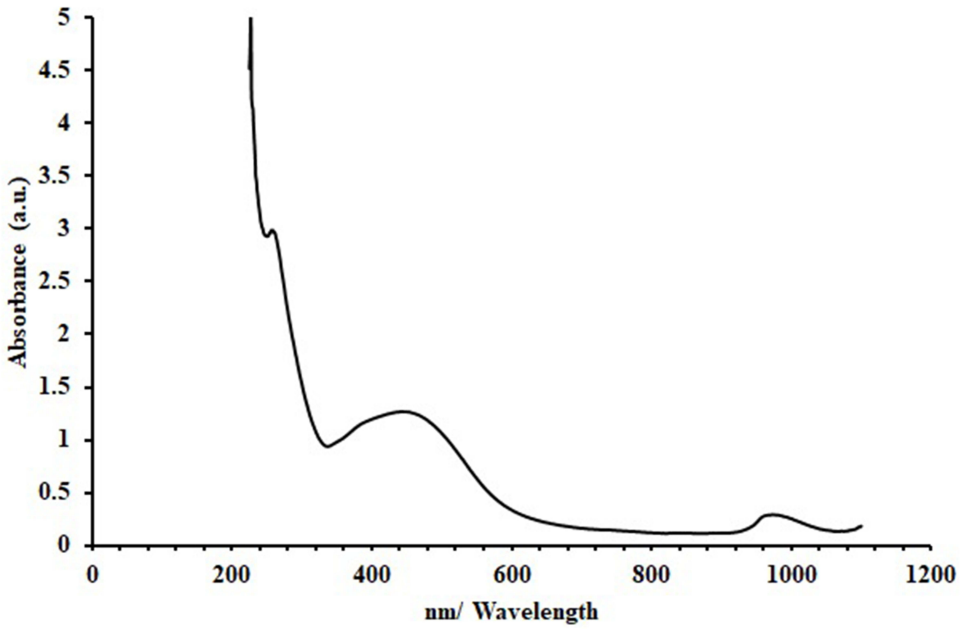

Figure 1 The UV-visible spectrum of an aqueous suspension of prepared AgNPs.

affected by the surfactant agent, the dielectric constant of the surrounding medium, and the chemicals adsorbed on the surface.[35,36]

Emission from silver nanoparticles is caused by the recombination of electron-hole pairs between the d-band and the sp-conduction band above the Fermi level,[37,38] which occurs at a credible 421.3nm when stimulated by 320 nm light. Emission intensity is increased in part because of the material absorbed during the formation of silver nanoparticles. Figure 2 depicts silver nanoparticles' photoluminescence (PL) spectrum when the excitation wavelength ranges from 400

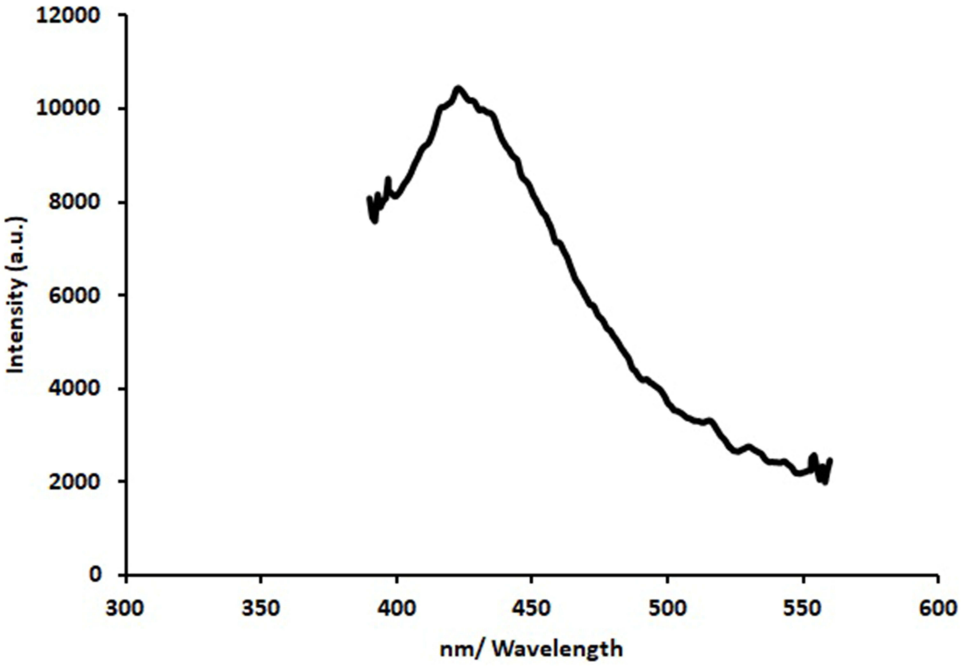

Figure 2 PL spectrum of prepared Ag NPs.

to 700 nm. The illumination of silver may be triggered by irradiating the metal surface with an electron, photon, or laser beam; the proven emission peak locations range from 300 to 550 nm.[39,40]

Nanoparticles, whose diameters are orders of magnitude smaller than the wavelength of light, are generally accepted to behave as dipoles in an optical field. About this dipole limit, nanoparticle absorption and emission should primarily be coherent with their surface excited energy bands or active surface sites.[41,42] Metal nanoparticle luminescence is explained by a variety of mechanisms; all of these mechanisms involve the photoelectron in the surface energy states strongly absorbing light at its plasmon resonance frequency and converting a portion of that energy into heat. A wavelength similar to that of the absorbed light is emitted.[34]

Dynamic light scattering (DLS) was used to analyse the particle size distribution of green AgNPs by determining their average hydrodynamic diameters and Polydispersity index (PdI). The DLS results showed a bimodal size distribution for the suspended particles, with the most prominent intensity peak at 104.3, 32.99 nm and the Z-average particle size at 93.38 nm. Figure 3 shows the particles' PdI to be 0.100. Extremely monodisperse, PdI values fall in the 0.1–0.2 range, whereas moderately polydisperse PdI values range from 0.1–0.4, and extremely polydisperse PdI values are over 0.4. Particle dispersity index (PdI) measures the variability in particle size distribution within a given sample. It is also known as the dispersity index or the heterogeneity index.[43,44]

The synthesized AgNPs are analyzed for their shape and particle size distribution using TEM. The synthesized nanoparticles' structural morphology exhibited clear signs of anisotropy– non-spherical structures (eg, prisms, rods, cubes) in nature[45] (Figure 4-left), and it also had crystalline features, which were represented by discrete lattice fringes (inset) (Figure 4-right). The decline in the efficiency of the reducing agents present in the plant extract was the primary factor in determining the shape of the nanoparticles. On nanoparticle surfaces, dark caps indicate secondary materials. It may be due to biomolecules found in the leaf extract.[26]

Several parameters, as reported by Rauwel, Molina, Parvataneni, and coworkers, may influence green-synthesized nanoparticles' size and form distribution. The variables reported are plant extract type, solution pH, and reaction temperature. The leaf extract decreased silver ions and shielded them from aggregation because the biomolecules act as protective agents. The biomolecules, however, reduce agents at higher levels of extract.[46–48]

Green synthetic AgNPs were analyzed for their elemental makeup using EDX. Elementary silver was found to have an EDX spectral peak at 3 keV (Figure 5). The optical absorption peak of silver nanocrystals is generally located around

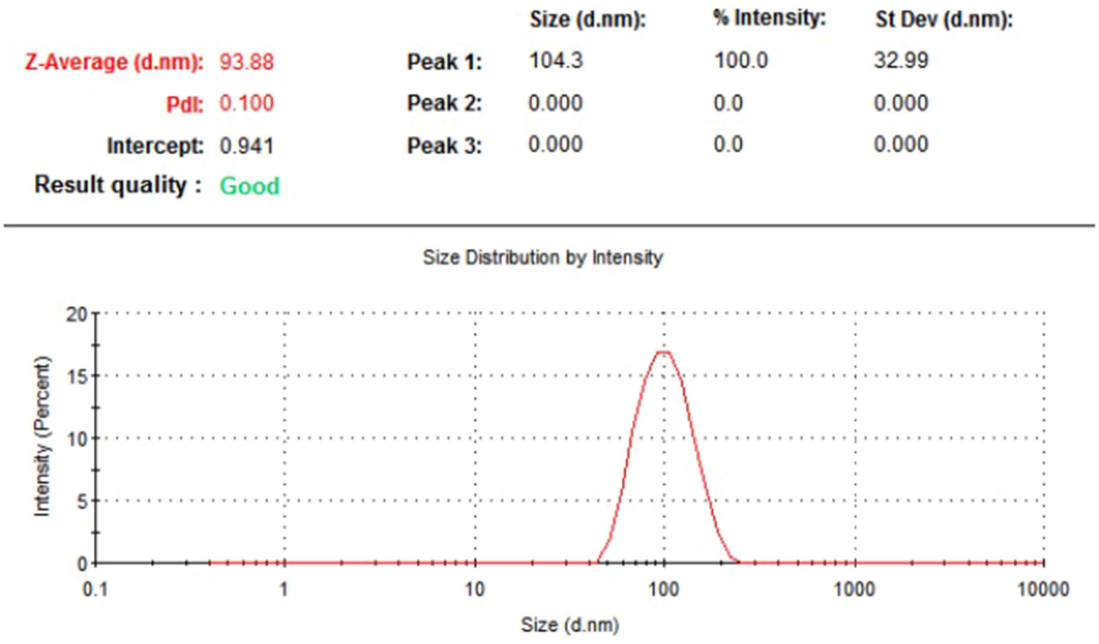

Figure 3 DLS obtained quantitative and qualitative profiles of green synthesized AgNPs.

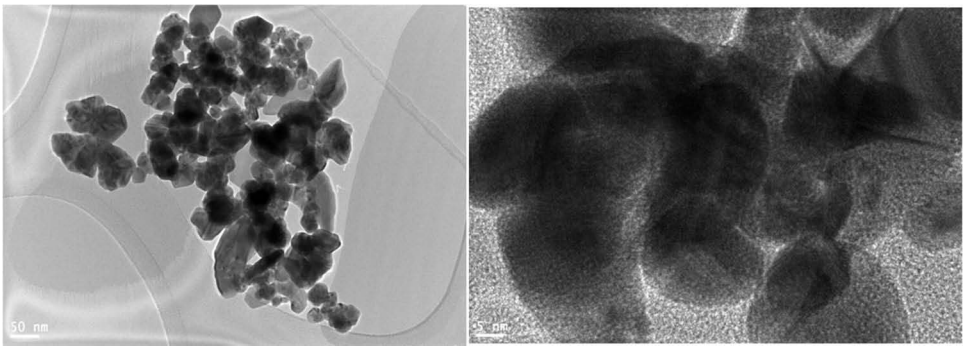

Figure 4 TEM micrographs of AgNPs (left) and distinct lattice fringes (inset) (right).

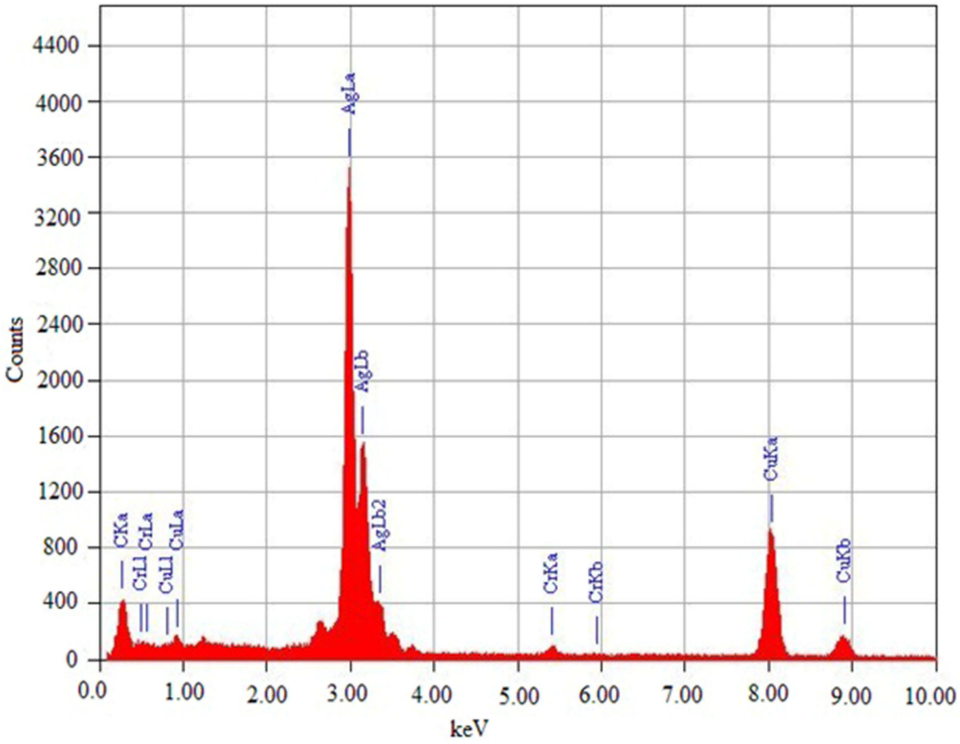

Figure 5 EDX pattern profile of synthesised AgNPs.

3 keV due to SPR. This confirms that AgNPs were synthesized and Ag+ was reduced to elemental silver.[49] Optical absorption peaks at 5.4 keV for Cr (Ka), 5.9 keV for Cr (Kb), and 0.5 keV for O (Ka) were evident due to other existing elements. Most plant and animal tissues contain this element but in low amounts. At the same time, the other signals are for copper since the FE-TEM uses a copper grid[50]. These components, which serve as protective coatings for AgNPs, are hypothesized to have originated in the plant extract. These findings are consistent with those from the EDX spectrum, which showed the existence of elemental silver and other metals during synthesis.[51,52]

FTIR spectroscopy was used to separate the functional groups of AgNPs within the scan ranges of 4000–400 cm^{-1}. According to the FTIR absorption bands (peaks) shown in Figure 6. The FTIR spectrum shows the existence of the (Ag) stretching vibration mode as metal-oxygen (M-O) due to the emergence of the transmission peak at 804.53 and 615.95 cm^{-1}. The area between 300 and 900 cm^{-1} has the highest stretching vibration concentration, as suggested.[53,54]

In order to determine the potential functional groups on the surfaces of the biosynthesized Ag nanoparticles, FTIR analysis was conducted. The results were compared to the FTIR spectrum of leaf extract, as shown in Figure 6. Looking

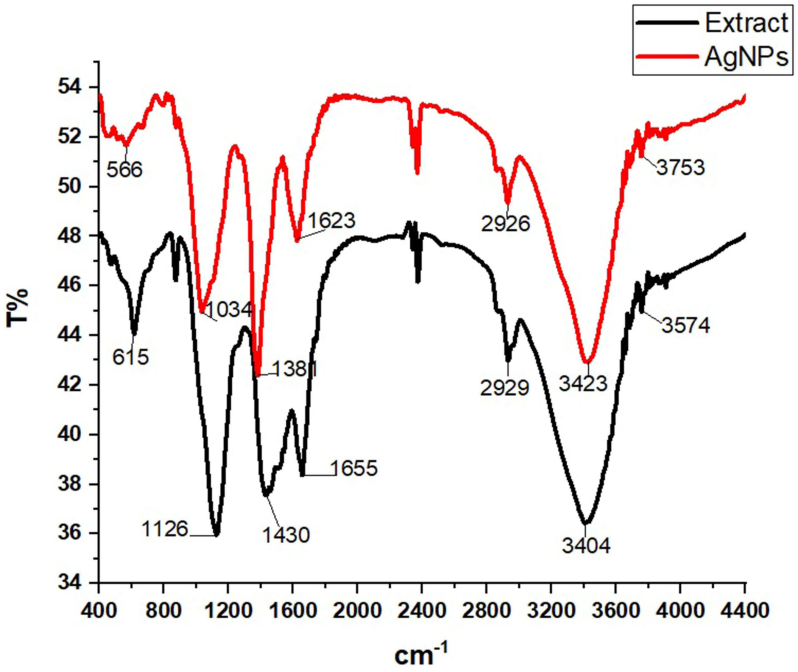

Figure 6 FTIR spectra of green synthesised AgNPs and N. procumbens extract.

back at Figure 6 a, it can be seen that the C-H bend pattern for alkenes peaks can be detected at 566 cm^{-1}, peaks observed around 1034 and 1381 cm^{-1} assigned to C–O stretching and C–H, which possibly the existence of CHO functional groups of carbohydrate. The band appeared at 1623 cm^{-1} assigned to the amide I and amide II region. The peaks at wave numbers around 2926, 34,234 and 3753 cm^{-1} were corresponding to stretching vibrations of C–H and N–H groups and OH groups of alcohol/phenol respectively. These findings are consistent with a prior investigation conducted.[55,56]

Tables 1, 2, and Figure 7 provide the findings of the disc diffusion approach used for the antibacterial evaluation of the green-synthesized AgNPs. *E. coli, S. aureus, E. faecalis, B. cereus, F. oxysporum, A. alternata, and Trichoderm*a were some of the clinical pathogens that were tested in this work to determine the activity of AgNPs that were synthesized using "green" technique.[57] The plant extract and AgNPs were tested for their antibacterial efficacy against a variety of bacterial (including Gram-negative *Escherichia coli and Gram-positive Staphylococcus aureus and Bacillus cereus strains)* and fungal (*including F. oxysporum, A. alternata, and Trichoderma)* strains using analysis of variance. The findings showed that the antibacterial action of AgNPs was substantially ($p \leq 0.05$) more evident against *Gramme-positive strains(S. aureus and B. cereus)* than *E. coli*, as shown in Figure 7 and Table 1. The diameter (mm) of the zone of inhibition caused by the biosynthesized Ag-NPs was substantially ($p \leq 0.05$) more significant than that caused by the

Table 1 The Measurement of Diameter (mm) of Inhibition Zones at Different Concentrations of Synthesized AgNPs Against Different Strains of Bacteria

Concentration of AgNPs (µL)	*S.auros*	*Bacillus cereus*	*E.coli*
1000	$19.67\pm0.577^{d*}$	$19.00\pm0.00^{d*}$	$10.00\pm0.00^{d*}$
500	$13.00\pm0.000^{c*}$	9.33 ± 0.577^{c}	8.67 ± 0.577^{c}
250	$8.67\pm0.577^{b*}$	4.00 ± 0.00^{b}	3.33 ± 0.577^{b}
N. procumbens extract	$5.00\pm0.000^{a*}$	0.33 ± 0.577^{a}	0^{a}

Notes: Different letters were used if there was a significant ($p \leq 0.05$) difference between the treatments and bacterial strains, then we consider the results to be meaningful. When there was a (*) significant ($p \leq 0.05$) difference between the strains and concentrations, we indicated it with a different letter (a, b, c or d).

Table 2 The Measurement of Diameter (mm) of the Zone of Inhibition at Different Concentrations of Synthesized AgNPs Against Different Fungal Strains

Concentration of AgNPs (µL)	A.alternata	Trichoderma	F. oxysporum
1000	18.33±0.577^{c*}	30.33±0.577^{c*}	25.00±1.00^{c*}
500	7.33±0.577^{b*}	15.00±0.00^{b*}	18.33±0.577^{b*}
N. procumbens extract	2.67±0.577^{a*}	8.67±0.577^{a*}	13.33±1.007^{a*}

Notes: There is a significant (p≤0.05) difference between the treatments for each fungal strain, as shown by using different letters (a, b, or c). (*) indicates a significant ($p \leq 0.05$) difference within different fungi strains for each concentration.

N. procumbens extract for all three concentrations tested (1000, 500, and 250 L). In addition, the biosynthesized Ag-NPs exhibited dose-dependent antibacterial action, consistent with a prior work by Awad et al.[48] The highest diameter of the inhibition zone was observed at 1000 µL of AgNPs against *S. aureus*((19.67±0.577mm) followed by *B. cereus*(19.00 ±0.00mm), which were both significantly ($p \leq 0.05$) higher than *E.coli* (10.00±0.00mm)(Table 1).

Furthermore, the biocidal activity of AgNPs against the fungal strains used in the study is shown in Table 1. For all three fungal strains, *A. alternata and Trichoderma*, and *F. oxysporum*, both the concentrations (1000 and 500 µL) of the biosynthesized Ag-NPs caused an inhibitory zone with a significantly (p≤0.05) higher diameter (in mm) than N. procumbens extract. In addition, biosynthesised Ag-NPs showed antifungal activity that increased with dosage. Among all three fungal strains used in the study, the *N. procumbens* extract and the AgNPs at both concentrations showed a significantly ($p \leq 0.05$) lower diameter of the zone of inhibition against *A.alternata* in comparison to *Trichoderma* and *F. oxysporum*. At the lower concentration (500 µL) of the AgNPs, the diameter was significantly ($p \leq 0.05$) higher for *F. oxysporum* (18.33±0.577mm) compared with *Trichoderma* (15.00±0.00mm) and *A.alternata* (7.33 ±0.577mm). However, at the higher concentration (1000 µL) of AgNPs, the highest diameter was recorded for *Trichoderma* (30.33±0.577mm), which was significantly higher than those recorded for *A. alternata and F. oxysporum* (Table 2).

The ability of AgNPs to produce silver ions, which are toxic to microbial cells, has been credited with a wide range of reported inhibitory mechanisms. The released Ag ions might damage the cell envelope by increasing membrane permeability after adhering to the cell wall and membrane. Additionally, silver ion adhesion can improve microbial cells and inactivate respiratory enzymes, increase the production of reactive oxygen species (ROS), halt the production of ATP, react with phosphorus and sulphur in DNA to block replication, halt cell division, and denature ribosome, inhibiting

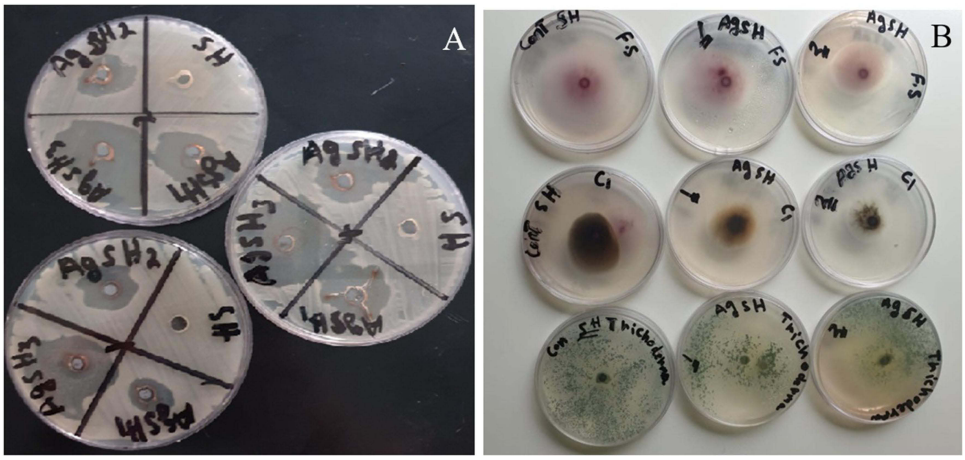

Figure 7 Observable clear zones produced by green synthesised AgNPs and N. procumbens extract against cultured pathogens: (**A**) gram-positive and gram-negative bacteria and (**B**) fungi evaluated by agar well diffusion assay.

protein synthesis. The second mode of inhibition involves the accumulation of AgNPs in the pits on the cell wall after they have penetrated the cell membrane, therefore modifying or destroying the structure of the cell wall and the cell membrane and causing the demise of the cell components. Gram-negative bacteria are more susceptible to AgNPs than Gram-positive bacteria due to variations in their cell wall composition. Gram-positive bacteria, which have more peptidoglycan in their cell membrane, have a more substantial cell wall than Gram-negative bacteria. Because of their thicker cell walls, gram-positive bacteria may be less susceptible to the inhibiting effects of AgNPs.[58–61]

MTT Assay Results

The inhibitory effect of the *N. procumbens* extract without and with NPs has been observed in vitro on *cervix adenocarcinoma* (Hela) and *breast adenocarcinoma* (MCF-7) cancer cells using the MTT test. Lower concentrations of the NPs (5–10µL) slightly reduced cell viability in both cells as compared to extract as a control (Figure 8). At higher concentrations (15–100µL) of plant extract with NPs, we decreased cell viability by more than 50% in both cells. The inhibition of cell viability is concentration dependent in both cells. Both plant extracts and synthesized nanoparticles showed more toxicity on MCF-7 cells than on Hela cells (Figure 8).

In most cases, the viability of the Hela and MCF-7 cells was reduced by nanoparticles in a dose-dependent manner, as depicted in Figure 9. In particular, at a concentration of 20 L, the treatment of both cell line cultures with extract did not induce cell death; however, it remarkably decreased cell viability for as-prepared AgNPs at 5 µL and higher doses, as illustrated in Figure 8. Interestingly, under the conditions tested, the cytotoxic impact of AgNPs was found to be the greatest among the two cell lines studied. Despite the lack of significant differences between Hela and MCF-7 cells, the extract was not toxic to the cells. The tested NPs showed more toxicity in MCF-7 cells than Hela (Figure 8). AgNPs synthesised from *Beta vulgaris* extract were previously reported to reduce cell viability when applied to the MCF-7, A549, and Hep2 cell lines in a dose-dependent manner. When leaf extract of *Andrographis echioides* was used to create AgNPs, they were tested against MCF-7 breast cancer cells, with the same outcomes.[62,63]

Several studies have shown that AgNPs can inhibit the growth of the human cancer cell lines MCF-7 and Hela including an extract from the *Eriobotrya japonica* plant.[64] Similar potent cytotoxicity and *anti-proliferative* activity were observed in AgNPs induced by Acer *oblongifolium* extract in MCF-7 and Hela cell lines.[65]

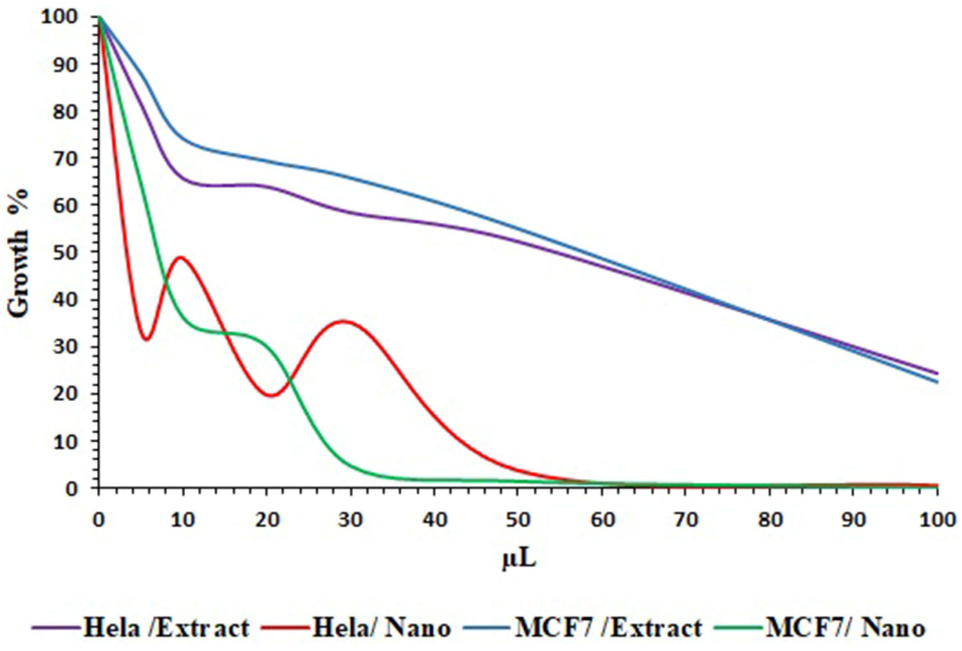

Figure 8 Cytotoxicity effect of N. procumbens extract without and within AgNPs in Hela and MCF-7 cell lines.

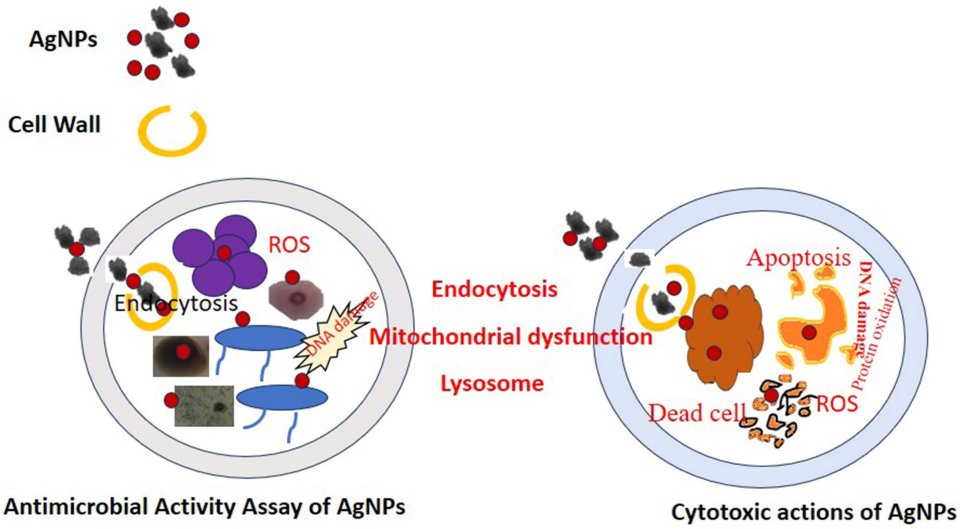

Figure 9 Mechanism of antimicrobial activity and cytotoxic action of AgNPs shown schematically.

Multiple studies have demonstrated the cytotoxic actions of metal NPs, but the intricate process by which they interact with live cells remains unclear, as shown in Figure 9. The ability of NPs to discharge metal ions into the cytosol and nucleus is well established. These ions quickly bind to the nitrogen bases and phosphate groups of DNA and the functional groups of proteins inside the cell, limiting their activity. This includes proteins that are inappropriately produced during cancer. However, it has been suggested that oxidative stress brought on by metal NPs is a critical component of their anticancer action. Noble metal NPs may cause a Fenton-like reaction, leading to reactive oxygen species, lipid and protein oxidation, DNA damage, and the activation of apoptosis, necrosis, and autophagy pathways, all of which lead to cell death.[66–68]

Conclusions

The following conclusions have been drawn from results and discussion. The produced AgNPs' UV-Vis spectra revealed a single absorption at 422 nm, suggesting that these nanoparticles are isotropic. The emergence of the transmission peak in the FTIR spectrum indicates the presence of the metal-oxygen (M-O) stretching vibration mode associated with Ag. The suspended particles' size distribution is bimodal, according to the DLS analysis, with the Z-average particle size measuring 93.38 nm and the most noticeable intensity peak occurring at 104.3, 32.99 nm.

According to TEM investigation, the green synthesised AgNPs containing N. promethens have a structural morphology that clearly shows anisotropy—non-spherical forms seen in nature, such as prisms, rods, and cubes.

The EDX spectral peak of elementary silver is determined to be at 3 keV. These results are consistent with the EDX spectrum, which shows the presence of additional metals including elemental silver throughout synthesis. The antimicrobial and cytotoxic properties of green-synthesized AgNPs are investigated. Many documented inhibitory mechanisms have been credited to AgNPs' capacity to produce silver ions, which are toxic to microbial cells. Furthermore, biosynthesized Ag-NPs exhibit increasing antifungal efficacy with dose.

Acknowledgments

The authors extend their appreciation to the Princess Nourah bint Abdulrahman University Researchers Supporting Project Number (PNURSP2024R47), Princess Nourah bint Abdulrahman University, Riyadh, Saudi Arabia.

Disclosure

The authors declare that they have no known competing financial interests or personal relationships that could have appeared to influence the work reported in this article.

References

1. Gautam YK, Sharma K, Tyagi S, Kumar A, Singh BP. Applications of green nanomaterials in coatings. *Green Nanoma Indus Applic*. 2022;107–152. doi:10.1016/b978-0-12-823296-5.00014-9
2. Ying S, Guan Z, Ofoegbu PC, et al. Green synthesis of nanoparticles: Current developments and limitations. *Environ Tech Inno*. 2022;26:102336. doi:10.1016/j.eti.2022.102336
3. Kharissova OV, Kharisov BI, Oliva González CM, Méndez YP, López I. Greener SYNTHESIS OF CHEMICAL COMPOUNDS AND MATERIALS. *Royal Soc Open Sci*. 2019;6:191378. doi:10.1098/rsos.191378
4. Parveen K, Banse V, Ledwani L Green synthesis of nanoparticles: their advantages and disadvantages. AIP Conference Proceedings, 2016.
5. Hano C, Abbasi BH. Plant-based green synthesis of nanoparticles: Production, characterization and applications. *Biomolecules*. 2021;12:31. doi:10.3390/biom12010031
6. Huang J, Xu Y, Xiao H, et al. Core–Shell Distinct Nanodrug Showing On-Demand Sequential drug release to act on multiple cell types for synergistic anticancer therapy. *ACS Nano*. 2019;13:7036–7049. doi:10.1021/acsnano.9b02149
7. Maaz K. *Silver Nanoparticles - Fabrication, Characterization and Applications*.InTech;2018,
8. Takáč P, Michalková R, Čižmáriková M, Bedlovičová Z, Balážová Ľ, Takáčová G. The role of silver nanoparticles in the diagnosis and treatment of cancer: are there any perspectives for the future? *Life*. 2023;13:466. doi:10.3390/life13020466
9. Gavas S, Quazi S, Karpiński TM. Nanoparticles for Cancer Therapy: current Progress and Challenges. *Nanoscale Res Lett*. 2021. doi:10.1186/s11671-021-03628-6
10. Thakur A, Thakur P, Khurana SMP. *Synthesis and Applications of Nanoparticles*.Springer Nature Singapore;2022.
11. Okafor F, Janen A, Kukhtareva T, Edwards V, Curley M. Green synthesis of silver nanoparticles, their characterization, application and antibacterial activity. *Int J Environ Res Public Health*. 2013;10:5221–5238. doi:10.3390/ijerph10105221
12. Martínez-Esquivias F, Guzmán-Flores JM, Perez-Larios A. antimicrobial activity of green synthesized Se Nanoparticles using ginger and onion extract: A laboratory and in silico analysis. *Part Sci Technol*. 2022;41:319–329. doi:10.1080/02726351.2022.2088432
13. Ahmed MJ, Murtaza G, Rashid F, Iqbal J. Eco-friendly green synthesis of silver nanoparticles and their potential applications as antioxidant and anticancer Agents. *Drug Dev Ind Pharm*. 2019;45:1682–1694. doi:10.1080/03639045.2019.1656224
14. Noorbazargan H, Amintehrani S, Dolatabadi A, et al. Anti-Cancer & anti-metastasis properties of bioorganic-capped silver nanoparticles fabricated from Juniperus chinensis extract against lung cancer cells. *AMB Express*. 2021;11. doi:10.1186/s13568-021-01216-6
15. Ovais M, Khalil AT, Raza A, et al. Green synthesis of silver nanoparticles via plant extracts: beginning a new era in cancer theranostics. *Nanomedicine*. 2016;11:3157–3177. doi:10.2217/nnm-2016-0279
16. Acharya D, Satapathy S, Somu P, Parida UK, Mishra G. Apoptotic effect and anticancer activity of biosynthesized silver nanoparticles from marine algae chaetomorpha linum extract against human colon cancer cell HCT-116. *Biol Trace Elem Res*. 2020;199:1812–1822. doi:10.1007/s12011-020-02304-7
17. Gomathi AC, Xavier Rajarathinam SR, Mohammed Sadiq A, Rajeshkumar S. Anticancer activity of silver nanoparticles synthesized using aqueous fruit shell extract of Tamarindus indica on mcf-7 human breast cancer cell line. *J Drug Deliv Sci Technol*. 2020;55:101376. doi:10.1016/j.jddst.2019.101376
18. Othman MM, Obeidat S, Al-Bagawi A, et al. Evaluation of the potential role of silver nanoparticles loaded with berberine in improving anti-tumor efficiency. *Pharm Sci*. 2021. doi:10.34172/ps.2021.28
19. Kumari K, Nandi A, Sinha A, et al. Biosurfactant-functionalized Silver nanoparticles infer intrinsic proximal interaction via Lysine and glutamic acid for reduced in vivo molecular biotoxicity with embryonic zebrafish through oxidative stress and apoptosis. *J Environ Chem Eng*. 2023;11(3):110147. doi:10.1016/j.jece.2023.110147
20. Sinha A, Simnani FZ, Singh D, et al. The translational paradigm of nanobiomaterials: biological chemistry to modern applications. *Mater Today Bio*. 2022;17:100463. doi:10.1016/j.mtbio.2022.100463
21. Panda PK, Kumari P, Patel P, et al. Molecular nanoinformatics approach assessing the biocompatibility of biogenic silver nanoparticles with channelized intrinsic steatosis and apoptosis. *Green Chem*. 2022;24(3):1190–1210. doi:10.1039/D1GC04103G
22. Husain S, Verma SK, Yasin D, Rizvi MMA, Fatma T. Facile green bio-fabricated silver nanoparticles from Microchaete infer dose-dependent antioxidant and anti-proliferative activity to mediate cellular apoptosis. *Bioor Chem*. 2021;107:104535. doi:10.1016/j.bioorg.2020.104535
23. Nasibova A. Generation of nanoparticles in biological systems and their application prospects. *Adv Biol Earth Sci*. 2023;8(2):140–146.
24. Baran A, Fırat Baran M, Keskin C, et al. Investigation of antimicrobial and cytotoxic properties and specification of silver nanoparticles (AgNPs) derived from Cicer arietinum L. green leaf extract. *Front Bioeng Biotech*. 2022;10:855136. doi:10.3389/fbioe.2022.855136
25. Ramazanli VN, Ahmadov IS. Synthesis of silver nanoparticles by using extract of olive leaves. *Adv Biol Ear Sci*. 2022;7(3):238–244.
26. Alharbi FA, Alarfaj AA. Green synthesis of silver nanoparticles from Neurada procumbens and its antibacterial activity against multi-drug resistant microbial pathogens. *J King Saud Univ Sci*. 2020;32(2):1346–1352.
27. Veisi H, Hemmati S, Shirvani H, Veisi H. Green synthesis and characterization of monodispersed silver nanoparticles obtained using oak fruit bark extract and their antibacterial activity. *Appl. Organo Chem*. 2016;30:387–391. doi:10.1002/aoc.3444
28. Quinten M, Leitner A, Krenn JR, Aussenegg FR. Electromagnetic Energy Transport via Linear Chains of Silver Nanoparticles. *Optics Lett*. 1998;23:1331. doi:10.1364/ol.23.001331
29. Wu F, Zhu J, Li G, et al. Biologically Synthesized Green Gold Nanoparticles from Siberian Ginseng Induce Growth-Inhibitory Effect on Melanoma Cells (B16). *Artif Cells Nano Biotech*. 2019;47:3297–3305. doi:10.1080/21691401.2019.1647224
30. Saha P, Kim BS. Plant extract and agricultural waste-mediated synthesis of silver nanoparticles and their biochemical activities. *Green Synth Silver Nanomat*. 2022;285–315. doi:10.1016/b978-0-12-824508-8.00010-1
31. Fayaz M, Tiwary CS, Kalaichelvan PT, Venkatesan R. Blue Orange Light Emission from Biogenic Synthesized Silver Nanoparticles Using Trichoderma Viride. *Colloids Surf B*. 2010;75:175–178. doi:10.1016/j.colsurfb.2009.08.028
32. Sastry M, Patil V, Sainkar SR. Electrostatically controlled diffusion of carboxylic acid derivatized silver colloidal particles in thermally evaporated fatty amine films. *J Phys Chem A*. 1998;102:1404–1410. doi:10.1021/jp9719873
33. Henglein A. Physicochemical properties of small metal particles in solution: "Microelectrode" Reactions, chemisorption, composite metal particles, and the atom-to-metal Transition. *J Phys Chem*. 1993;97:5457–5471. doi:10.1021/j100123a004

34. Mishra YK, Mohapatra S, Kabiraj D, et al. Synthesis and characterization of ag nanoparticles in silica matrix by atom beam sputtering. *Scr Mater*. 2007;56:629–632. doi:10.1016/j.scriptamat.2006.12.008
35. Chugh D, Viswamalya VS, Das B. Green synthesis of silver nanoparticles with algae and the importance of capping agents in the process. *J Genet Eng Biotechnol*. 2021. doi:10.1186/s43141-021-00228-w
36. Ortega-Arroyo L, Martin-Martinez ES, Aguilar-Mendez MA, Cruz-Orea A, Hernandez-Pérez I, Glorieux C. Green synthesis method of silver nanoparticles using starch as capping agent applied the methodology of surface response. *Starch*. 2013;65:814–821. doi:10.1002/star.201200255
37. Gangopadhyay P, Kesavamoorthy R, Bera S, et al. Optical absorption and photoluminescence spectroscopy of the growth of silver nanoparticles. *Phys Rev Lett*. 2005;94. doi:10.1103/physrevlett.94.047403
38. Bhagat M, Anand R, Datt R, Gupta V, Arya S. Green synthesis of silver nanoparticles using aqueous extract of rosa brunonii lindl and their morphological, biological and photocatalytic characterizations. *J Inorg Organomet Polym Mater*. 2018;29:1039–1047. doi:10.1007/s10904-018-0994-5
39. Zahran M, El-Kemary M, Khalifa S, El-Seedi H. Spectral studies of silver nanoparticles biosynthesized by origanum Majorana. *Green Proc Synthesis*. 2018;7:100–105. doi:10.1515/gps-2016-0183
40. Zhang A, Zhang J, Fang Y. Photoluminescence from colloidal silver nanoparticles. *J Lumin*. 2008;128:1635–1640. doi:10.1016/j.jlumin.2008.03.014
41. Mondal K, Biswas S, Singha T, Chatterjee U, Datta PK, Kumbhakar P. Enhanced optical power limiting and visible luminescence in colloidal dispersion of ultra-small au nanoclusters Synthesized by Single-Pot Chemical Technique. *J Mol Liq*. 2021;322:114909. doi:10.1016/j.molliq.2020.114909
42. Chen S, Ingram RS, Hostetler MJ, et al. Gold nanoelectrodes of varied size: transition to molecule-like charging. *Science*. 1998;280:2098–2101. doi:10.1126/science.280.5372.2098
43. Bhattacharjee S. DLS and zeta potential – what they are and what they are not? *J Control Release*. 2016;235:337–351. doi:10.1016/j.jconrel.2016.06.017
44. de Carvalho Bernardo WL, Boriollo MFG, Tonon CC, et al. Antimicrobial effects of silver nanoparticles and extracts of Syzygium cumini flowers and seeds: Periodontal, Cariogenic and Opportunistic Pathogens. *Arch Oral Biol*. 2021;125:105101. doi:10.1016/j.archoralbio.2021.105101
45. Pearce AK, Wilks TR, Arno MC, O'Reilly RK. Synthesis and applications of anisotropic nanoparticles with precisely defined dimensions. *Nature Rev Chem*. 2020;5:21–45. doi:10.1038/s41570-020-00232-7
46. Rauwel P, Küünal S, Ferdov S, Rauwel E. A review on the green synthesis of silver nanoparticles and their Morphologies studied via TEM. *Ad. Mater Sci Eng*. 2015;1–92015
47. Parvataneni R. Biogenic Synthesis and Characterization of Silver Nanoparticles Using Aqueous Leaf Extract of Scoparia Dulcis L. and Assessment of Their Antimicrobial Property. *Drug Chem Toxicol*. 2019;43:307–321. doi:10.1080/01480545.2018.1505903
48. Jyoti K, Baunthiyal M, Singh A. Characterization of Silver Nanoparticles Synthesized Using Urtica Dioica Linn. Leaves and Their Synergistic Effects with Antibiotics. *J Radiat Res Appl Sci*. 2016;9:217–227. doi:10.1016/j.jrras.2015.10.002
49. Huq M. Green Synthesis of Silver Nanoparticles Using Pseudoduganella Eburnea MAHUQ-39 and Their Antimicrobial Mechanisms Investigation against Drug Resistant Human Pathogens. *Int J Mol Sci*. 2020;21:1510. doi:10.3390/ijms21041510
50. Meer D, Naidoo S, Dewir YH, Lin Y, Rihan JZ. Green synthesis of silver nanoparticles from heteropyxis natalensis leaf extract and their potential antibacterial efficacy. *ScienceAsia*. 2022;48:196. doi:10.2306/scienceasia1513-1874.2022.039
51. Shaik M, Khan M, Kuniyil M, et al. Plant-extract-assisted green synthesis of silver nanoparticles using Origanum vulgare L. *Extra Microbl Act Sustain*. 2018;10:913. doi:10.3390/su10040913
52. Bratovcic A. Synthesis, Characterization, Applications, and Toxicity of Lead Oxide Nanoparticles. *Lead Chemistry*. 2020. doi:10.5772/intechopen.91362
53. Dang-Bao T, Hoang Bao N, Phung Anh N, Hong Phuong P, Nguyen TT, Tri N. Green-synthesized silver nanoparticles decorated on ceria nanorods for room-temperature p-nitrophenol hydrogenation. *Green Chem Lett Rev*. 2022;15(2):449–459. doi:10.1080/17518253.2022.2089060
54. Tailor G, Lawal AM. Phytochemical Screening; Green Synthesis, Characterization and Biological Significance of Lead Oxide Nanoparticles from Eucalyptus Globulus Labill. *Nanotech Environl Eng*. 2021;6. doi:10.1007/s41204-021-00143-y
55. Gole A, Dash C, Ramakrishnan V, et al. Pepsin− gold colloid conjugates: preparation, characterization, and enzymatic activity. *Langmuir*. 2001;17(5):1674–1679. doi:10.1021/la001164w
56. Maniraj A, Kannan M, Rajarathinam K, Vivekanandhan S, Muthuramkumar S. Green synthesis of silver nanoparticles and their effective utilization in fabricating functional surface for antibacterial activity against multi-drug resistant Proteus mirabilis. *Journal of Cluster Science*. 2019;30:1403–1414. doi:10.1007/s10876-019-01582-z
57. Awad MA, Eisa NE, Virk P, et al. Green synthesis of gold Nanoparticles: Preparation, characterization, cytotoxicity, and anti-bacterial activities. *Mater Lett*. 2019;256:126608. doi:10.1016/j.matlet.2019.126608
58. Fouda A, Awad MA, AL-Faifi ZE, et al. Aspergillus Flavus-Mediated Green Synthesis of Silver Nanoparticles and Evaluation of Their Antibacterial, Anti-Candida, Acaricides, and Photocatalytic Activities. *Catalysts*. 2022;12:462. doi:10.3390/catal12050462
59. Salem SS, Fouda A. Green Synthesis of Metallic Nanoparticles and Their Prospective Biotechnological Applications: an Overview. *Biol Trace Elem Res*. 2020;199:344–370. doi:10.1007/s12011-020-02138-3
60. El-Belely EF, Farag MMS, Said HA, et al. Green Synthesis of Zinc Oxide Nanoparticles (ZnO-NPs) Using Arthrospira Platensis (Class: cyanophyceae) and Evaluation of Their Biomedical Activities. *Nanomaterials*. 2021;11:95. doi:10.3390/nano11010095
61. Yin IX, Zhang J, Zhao IS, Mei ML, Li Q, Chu CH. The antibacterial mechanism of silver nanoparticles and its application in dentistry. *Int j Nanomed*. 2020;15:2555. doi:10.2147/IJN.S246764
62. Venugopal K, Ahmad H, Manikandan E, et al. The impact of anticancer activity upon Beta vulgaris extract mediated biosynthesized silver nanoparticles (AgNPs) against human breast (MCF-7), lung (A549) and pharynx (Hep-2) cancer cell lines. *J Photochem Photobiol B Biol*. 2017;173:99–107. doi:10.1016/j.jphotobiol.2017.05.031
63. Elangovan K, Elumalai D, Anupriya S, Shenbhagaraman R, Kaleena PK, Murugesan K. Phyto mediated biogenic synthesis of silver nanoparticles using leaf extract of Andrographis echioides and its bio-efficacy on anticancer and antibacterial activities. *J Photochem Photobiol B Biol*. 2015;151:118–124. doi:10.1016/j.jphotobiol.2015.05.015

64. Jabir MS, Hussien AA, Sulaiman GM, et al. Green synthesis of silver nanoparticles from Eriobotrya japonica extract: a promising approach against cancer cells proliferation, inflammation, allergic disorders and phagocytosis induction. *Artif. Cells Nanomed. Biotechnol.* 2021;49:48–60. doi:10.1080/21691401.2020.1867152
65. Naveed M, Bukhari B, Aziz T, et al. Green Synthesis of Silver Nanoparticles Using the Plant Extract of Acer oblongifolium and Study of Its Antibacterial and Antiproliferative Activity via Mathematical Approaches. *Molecules*. 2022;27:4226. doi:10.3390/molecules27134226
66. Saleem HD, Hamza TA, Izzat SE, Hamad DA, Abdulhasan MJ, Adhab AH. Role Silver and Bimetallic Nano Particles Synthesized by Green Chemical Methods for their Therapeutic Potential for Cancer: a Review. *J Pharml Quality Ass*. 2022:2022
67. Alharbi NS, Alsubhi NS, Felimban AI. Green synthesis of silver nanoparticles using medicinal plants: characterization and application. *J Radiat Res Appl Sci*. 2022;15(3):109–124. doi:10.1016/j.jrras.2022.06.012
68. Rizwana H, Bokahri NA, Alfarhan A, Aldehaish HA, Alsaggabi NS. Biosynthesis and characterization of silver nanoparticles prepared using seeds of Sisymbrium irio and evaluation of their antifungal and cytotoxic activities. *Green Proces Synthesis*. 2022;11(1):478–491. doi:10.1515/gps-2022-0048